Hittite Journal of Science and Engineering, 2021, 8(1) 01–05
ISSN NUMBER: 2148–4171
DOI: 10.17350/HJSE19030000206

Fabrication and Analysis Of 2D/3D Heterojunction Between Continuous Few-layer WS_2 Film and Si (100)†

Merve Acar[1] Soheil Mobtakeri[2] Mehmet Ertugrul[1] Emre Gur[2]
[1]Ataturk University, Department of Electrical and Electronics Engineering, Erzurum, Turkey
[2]Ataturk University, Department of Physics, Erzurum, Turkey

ABSTRACT

Transition metal dichalcogenide (TDMCs) placed on a 3D semiconductor substrate have leads to significant advances in the electronic industry with new opportunities based on 2D/3D heterojunction based diverse devices without any restrictions, such as lattice compatibility. In this study, magnetron sputtering technique was used to grow layered tungsten disulfide (WS_2) thin films onto p-Si and thus WS_2/p-Si heterojunctions were created. The structural and chemical parameters of this sputtered WS_2 films were investigated using Raman spectroscopy, X-ray photoelectron spectroscopy (XPS) and atomic force microscopy (AFM). Electrical characterization of WS_2/p-Si heterojunction was also obtained to investigate Log (I)-V and linear I-V characteristics. A typical diode like I-V behavior was observed with a five-ordered rectifying ratio. It was observed that the heterojunction has a barrier height of 0.48 eV, the leakage current at -0.2 V is 2.25×10^{-6} A and the ideality factor is 5.7. This work show that single step magnetron sputtering WS_2/p-Si heterojunction has great importance for heterojunction based future nanoelectronic devices.

Article History:
Received: 2020/05/30
Accepted: 2020/12/27
Online: 2021/03/31

***Correspondence to**: Emre Gür,*
Deparment of Electrical and Electronics Engineering, Atatürk University, Erzurum, Turkey
Tel: +90 442 136 6733
Fax: +90 442 236 0948
E-Mail:emregur@atauni.edu.tr

Keywords:
2D materials, TMDC, WS_2, 2D/3D heterojunctions

INTRODUCTION

The excellent electronic properties of the various two-dimensional (2D) materials have led to new developments for the nanoelectronic devices after discovering of the graphene. Heterostructures created by using 2D and 3D materials are becoming one of the main research area for the nanoelectronic devices in recent years [1]. TMDCs such as WS_2, MoS_2, $MoSe_2$, and WSe_2 have adjustable bandgaps to be indirect in their bulk form and direct in the monolayer [2]. This feature has potential in various electronic and optical applications for TMDCs [3]. Structurally, WS_2 has a crystal structure consisting of S-W-S sandwich layers and the atoms in the layers are packaged hexagonally [4]. These layers are held together by the weak van der Waals (vdW) forces so WS_2 can easily be converted into a single layer form [5]. Because of these significant features, WS_2 has become a good candidate for the new generation micro and nanoelectronics [6]. Unlike the graphene, the WS_2 has a direct band gap semiconductor with a gap of 2.1 eV in single layer form while as the material passes into a bulk form, the gap is direct in the size of 1.3 eV [7]. The presence of this bandgap made it possible to produce WS_2 transistors with a 10^8 on/off ratio and high sensitivity photo detectors [8].

Integration of TMDCs with 3D materials such as Si and GaN offers interesting opportunities. Lattice matching is very important in the integration of different bulk semiconductors [9, 10]. These heterojunction can be vertical and lateral structures, without lattice matching restrictions [11]. 2D vdW heterostructures offer unique features compared to TMDC devices. Recently, researchers have begun to study various heterojunction device based on 2D/3D materials [12].

MoS_2/Si heterojunctions have found used in high performance device applications such as photodetectors [13-15] and solar cells [16]. It has also been studied MoS_2/GaAs [17], MoS_2/InP [18], MoS_2/SiC [19, 20] and MoS_2/GaN heterojunctions [12, 16, 21-26] for a diverse applications. MoS_2/WSe_2 [27-29] and MoS_2/GaN [12, 25] heterojunctions based devices have also found a place in different electronic device applications. On the other hand, heterojunction based devices have also been carried out with 2D WS_2. WS_2/Si p-n junction was fabricated and rectifying characteristics was demonstrated [30]. GaN and WS_2 monolayers have the same crystal structures and lattice constants compatible with each other, WS_2/GaN junction was fabricated with wafer-

scale grown WS_2 film [31]. In another study, WS_2/GaN heterojunction was manufactured for UV detection [32].

Large area and continuous WS_2 thin film creation is a crucial step for nanoelectronic device production [33, 34]. WS_2 films can be prepared in two different ways: top-down or bottom-up. The top-down method contains exfoliation method (mechanical or chemical) is not suitable for commercialization, as is not possible to control the thickness and size of WS_2 films in this method [35]. The chemical vapor deposition (CVD) method from bottom-up methods is the most widely used method [36]. Although large area single crystal 2D graphene can be grown with this method. However, TMDC (MoS_2, WS_2) creation of wafer-scale single-layer films with the CVD method [37]. It is important to create the heterojunction with large area WS_2 thin films [38] and Si. Therefore, integration of WS_2 with Si, multifunctional devices can be realized. However, there are no studies on the production of heterojunctions composed of single step sputtered WS_2 thin films and Si.

In this study, the magnetron sputtering method was utilized to produce a continuous and centimeter size WS_2 film with a thickness of ~ 15 nm. WS_2 thin films were sputtered on p-type Si to produce 2D/3D heterojunctions.

MATERIAL AND METHODS

The resistivity of the highly doped p type silicon was used in this study to prepare WS_2/Si heterojunction. Before the fabrication of devices, Si substrates were cleaned by using RCA procedure. Afterward Si substrate rinsed in DI water and dried N_2 gas. The fabrication process WS_2/Si heterojunction is given step by step as shown in Fig. 1. Before the growth of WS_2 on Si, the Al was created on the unpolished side of the Si in a sputter system and p-Si/Al was annealed to achieve ohmic contact in N_2 gas flow at 540 ° C for 3 minutes. WS_2 thin continuous films were grown on p-Si (100) substrate for the 10s at 5×10-7 Torr base pressure and 20mTorr growth pressure. Substrate temperature and sputtering power were set to the 300 °C and 120 W respectively. Ar gas was adjusted as 220 sccm. Schematic diagram of deposition of WS_2 by magnetron sputtering is shown in Fig. 2. AZ5214 photoresist was coated for lithography and then exposed under UV light. Then, 5/50 nm thick Ti/Pt contacts were deposited on the WS_2 layer using sputtering at 10^{-6} Torr base pressure and 20mTorr growth pressure in Ar ambient. After coating, using lift-off process Ti/Pt contacts were created as square with dimensions of 150μ×150μ. For the electrical characterization DC voltage was applied to the top and bottom contacts at atmosphere condition.

Before the fabrication process, structural and chemical properties of the WS_2 layer were characterized using Raman spectroscopy (Witec Alfa-300), XPS (SPECs Flex-Mod) and AFM measurement.

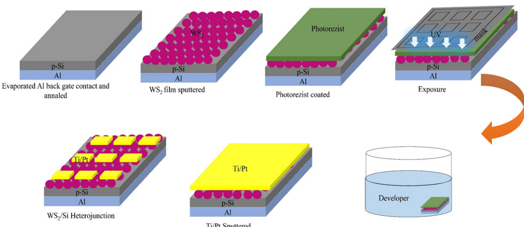

Figure 1. Schematic fabrication procedure of WS_2/Si heterojunction.

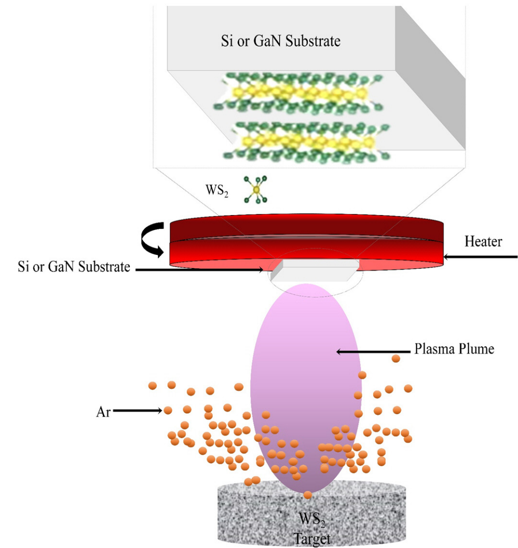

Figure 2. Schematic illustration of the sputtering process.

Once and for all, the current (I)-voltage (V) characteristics of WS_2/Si heterojunctions were determined using Keithley 2400 source meter at atmosphere condition.

RESULTS AND DISCUSSION

Raman spectroscopy used to sputtered growth WS_2 film. Fig. 3 shows the Raman spectrum of a few layers WS_2 films on p-Si substrates. The Raman two important modes, E^1_{2g} at 340, 4 cm^{-1} and A_{1g} at 406, 5 cm^{-1} of the grown multilayer WS_2 film. The peak difference between E^1_{2g} and A_{1g} mode Raman peaks are measured as 66.1 cm^{-1}, which demonstrates the presence of the multilayer WS_2 film [39].

Moreover, the surface morphology of the few layer WS_2 film on p-Si substrate is analyzed by optic microscope images and AFM characterizations, the results are shown in Fig. 4. In Fig. 4(a) 3D AFM images clearly show the step formed at the interface where WS_2 grown on p-Si. Drawn green line in Fig. 4(b) is show height profile of the surface. It can be seen from the Fig. 4(c) that the thickness of 10 s grown WS_2

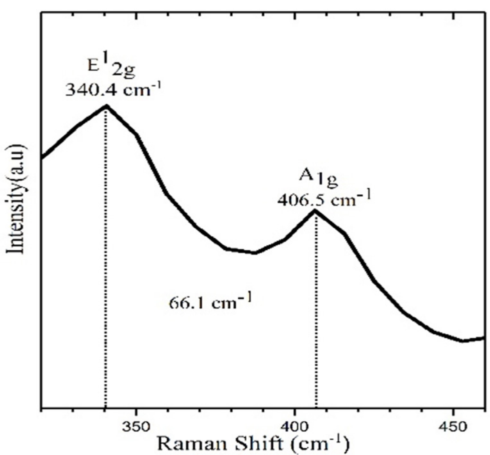

Figure 3. Raman spectrum of the grown continuous few layer WS_2 films on p-Si substrate.

film is 15 nm. Fig. 4(d) shows an optical microscope image of 2D WS_2 thin films where continuous and uniform films can be easily seen over a large area.

Chemical composition of the WS_2 film was analyzed with XPS measurement. XPS W 4f spectrum of WS_2 film is shown in figure 5(a). The peaks observed W $4_{f7/2}$ at 32.0 eV, W $4_{f5/2}$ at 34.8 eV and W $5_{p3/2}$ at 38 eV. Fig. 5(b) illustrates the S 2p spectra; the peaks identified S $2_{p3/2}$ at 162. 98 eV. Atomic ratio of the S/W is also determined from the XPS measurements as 1.38. These XPS result confirms that S deficient WS_2 films were successfully grown by sputtering.

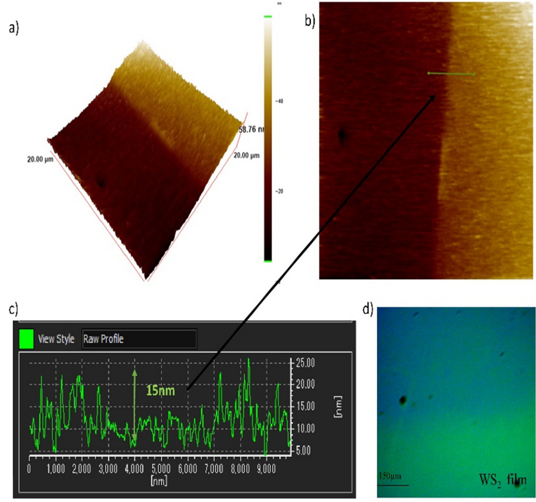

Figure 4. a) An AFM 3D image of few layer WS2 film. b) Large area scanned AFM image of the WS_2-Si interface. c) Height profile showing the thickness of WS_2 passing through the green line in b). d) An optical microscope image of a few layer continuous WS_2 film growth on p-Si substrate.

I-V measurements were performed under atmosphere conditions to evaluate the electrical properties of the WS_2/p-Si heterojunction. I-V graph of WS_2/p-Si heterojunction taken between -2 volts and +2 volts is given in Fig. 6. The linear and logarithmic I-V curve are shown in Fig. 6(a) and 6(b). Fig. 6(c) shows schematic representation of Al back gated WS_2/Si heterojunction with connections. The log I-V curves shows diode like rectifying characteristic with rectification ratio over 10^5 in the range of ±2V. Almost saturated I-V curve for reverse bias depicts the less interface effects at the junction. The leakage current is about 2.28×10^{-6} A at –0.2V was observed. The turn on voltage, which is the point where the current starts to increase rapidly, was observed at 0.5 V.

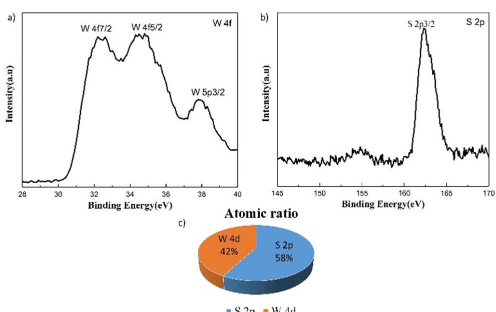

Figure 5. XPS spectrum of a) W 4f and b) S 2p spectrums of the WS_2 film on Si c) Atomic ratio of WS_2 film.

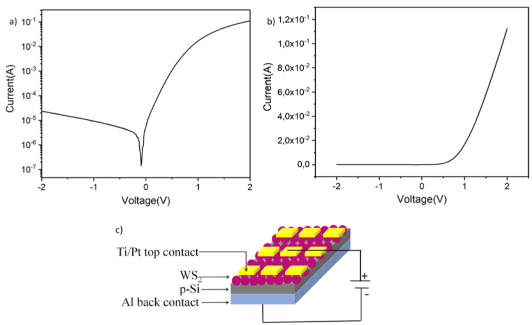

Figure 6. I–V characteristics of the heterojunction on a) logarithmic and b) linear scales in the atmosphere condition. c) Schematic representation of WS_2/Si heterojunction.

As in the metal-semiconductor contact of the WS_2/Si heterojunction, the carrier transport is mainly caused by minority charge carriers. But in this article, since Si is highly doped, it may work like a unilateral Schottky junction. Thermionic emission (TE) current equation can be used to calculate ideality factor (n) and barrier height (Φb). For this, the slope and intersection of the log I-V curve are used. The current passing through the WS_2/p-Si heterojunction as defined the theory of TE, as in the following Eq. 1:

$$I = I_0 \exp\left(\frac{qV}{nkT}\right)\left[1-\exp\left(-\frac{qV}{kT}\right)\right] \quad (1)$$

where q:electronic charge, v:applied voltage, T:temperature, k:Boltzmann constant, n:ideality factor, I_0:

reverse saturation current. The ideality factor (n) is calculated from forward bias linear region of the ln (I) -V graph using the following Eq. 2:

$$n = \frac{q}{kT}\left(\frac{dV}{d(lnI)}\right) \quad (2)$$

In addition, another important parameter, Barrier height (Φb), can be calculated using the Eq. 3 below.

$$\Phi b = \frac{kT}{q} In\left(\frac{AA^{*}T^{2}}{I_{0}}\right) \quad (3)$$

A: area and A*: effective Richardson constant (32 $Acm^{-2}K^{-2}$ for Si). Ideality factor (n) and barrier height (Φb) accounted for the WS_2/p-Si heterojunction according to the above equations, the corresponding values were 5.7 and 0.48 eV, respectively. The ideality factor value (n) is greater than 1 when there is the presence of interface layer or surface conditions, the effect of series resistance, the height of the barrier caused by interface defects and manufacturing defects. The larger ideality factor might show that current carrying mechanisms is other than thermionic emissions [40].

CONCLUSION

In summary, large-area and continuous few layer WS_2 films were synthesized on the p-Si by single step magnetron sputtering successfully. WS_2/Si heterojunction device was fabricated by lithography. Electrical measurements shows that the WS_2/Si heterojunction have remarkable rectifying behavior, around 10^5. This type heterojunctions might be advantageous for future nano and optoelectronic device applications.

REFERENCES

1. Jariwala, D.; Marks, T. J.; Hersam, M. C., Mixed-dimensional van der Waals heterostructures. Nature materials 2017, 16 (2), 170-181.
2. Liu, B. L.; Abbas, A.; Zhou, C. W., Two-Dimensional Semiconductors: From Materials Preparation to Electronic Applications. Adv Electron Mater 2017, 3 (7).
3. Shim, J.; Park, H. Y.; Kang, D. H.; Kim, J. O.; Jo, S. H.; Park, Y.; Park, J. H., Electronic and Optoelectronic Devices based on Two-Dimensional Materials: From Fabrication to Application. Adv Electron Mater 2017, 3 (4).
4. Choi, W.; Choudhary, N.; Han, G. H.; Park, J.; Akinwande, D.; Lee, Y. H., Recent development of two-dimensional transition metal dichalcogenides and their applications. Mater Today 2017, 20 (3), 116-130.
5. Sumesh, C. K., Temperature dependant electronic charge transport characteristics at MX2 (M=Mo,W; X=S, Se)/Si heterojunction devices. J Mater Sci-Mater El 2019, 30 (4), 4117-4127.
6. Wang, Q. H.; Kalantar-Zadeh, K.; Kis, A.; Coleman, J. N.; Strano, M. S., Electronics and optoelectronics of two-dimensional transition metal dichalcogenides. Nature nanotechnology 2012, 7 (11), 699.
7. Ahmed, S.; Yi, J., Two-dimensional transition metal dichalcogenides and their charge carrier mobilities in field-effect transistors. Nano-Micro Lett 2017, 9 (4), 50.
8. Ye, M.; Zhang, D.; Yap, Y. K., Recent advances in electronic and optoelectronic devices based on two-dimensional transition metal dichalcogenides. Electronics 2017, 6 (2), 43.
9. Dong, R.; Kuljanishvili, I., Progress in fabrication of transition metal dichalcogenides heterostructure systems. Journal of Vacuum Science & Technology B, Nanotechnology and Microelectronics: Materials, Processing, Measurement, and Phenomena 2017, 35 (3), 030803.
10. Gupta, P.; Rahman, A.; Subramanian, S.; Gupta, S.; Thamizhavel, A.; Orlova, T.; Rouvimov, S.; Vishwanath, S.; Protasenko, V.; Laskar, M. R., Layered transition metal dichalcogenides: promising near-lattice-matched substrates for GaN growth. Sci Rep-Uk 2016, 6, 23708.
11. Wang, J. W.; Li, Z. Q.; Chen, H. Y.; Deng, G. W.; Niu, X. B., Recent Advances in 2D Lateral Heterostructures. Nano-Micro Lett 2019, 11 (1).
12. O'Regan, T. P.; Ruzmetov, D.; Neupane, M. R.; Burke, R. A.; Herzing, A. A.; Zhang, K.; Birdwell, A. G.; Taylor, D. E.; Byrd, E. F.; Walck, S. D., Structural and electrical analysis of epitaxial 2D/3D vertical heterojunctions of monolayer MoS2 on GaN. Appl Phys Lett 2017, 111 (5), 051602.
13. Li, B.; Shi, G.; Lei, S.; He, Y.; Gao, W.; Gong, Y.; Ye, G.; Zhou, W.; Keyshar, K.; Hao, J., 3D band diagram and photoexcitation of 2D–3D semiconductor heterojunctions. Nano Lett 2015, 15 (9), 5919-5925.
14. Krishnamoorthy, S.; Lee, E. W.; Lee, C. H.; Zhang, Y.; McCulloch, W. D.; Johnson, J. M.; Hwang, J.; Wu, Y.; Rajan, S., High current density 2D/3D MoS2/GaN Esaki tunnel diodes. Appl Phys Lett 2016, 109 (18), 183505.
15. Esmaeili-Rad, M. R.; Salahuddin, S., High performance molybdenum disulfide amorphous silicon heterojunction photodetector. Sci Rep-Uk 2013, 3 (1), 1-6.
16. Hao, L.; Liu, Y.; Gao, W.; Han, Z.; Xue, Q.; Zeng, H.; Wu, Z.; Zhu, J.; Zhang, W., Electrical and photovoltaic characteristics of MoS2/Si pn junctions. J Appl Phys 2015, 117 (11), 114502.
17. Hao, L.; Liu, Y.; Han, Z.; Xu, Z.; Zhu, J., Large lateral photovoltaic effect in MoS 2/GaAs heterojunction. Nanoscale research letters 2017, 12 (1), 562.
18. Lin, S.; Wang, P.; Li, X.; Wu, Z.; Xu, Z.; Zhang, S.; Xu, W., Gate tunable monolayer MoS2/InP heterostructure solar cells. Appl Phys Lett 2015, 107 (15), 153904.
19. Lee, E. W.; Ma, L.; Nath, D. N.; Lee, C. H.; Arehart, A.; Wu, Y.; Rajan, S., Growth and electrical characterization of two-dimensional layered MoS2/SiC heterojunctions. Appl Phys Lett 2014, 105 (20), 203504.
20. Din, H.; Idrees, M.; Rehman, G.; Nguyen, C. V.; Gan, L.-Y.; Ahmad, I.; Maqbool, M.; Amin, B., Electronic structure, optical and photocatalytic performance of SiC–MX 2 (M= Mo, W and X= S, Se) van der Waals heterostructures. Phys Chem Chem Phys 2018, 20 (37), 24168-24175.
21. Zhang, K.; Jariwala, B.; Li, J.; Briggs, N. C.; Wang, B.; Ruzmetov, D.; Burke, R. A.; Lerach, J. O.; Ivanov, T. G.; Haque, M., Large scale 2D/3D hybrids based on gallium nitride and transition metal dichalcogenides. Nanoscale 2018, 10 (1), 336-341.
22. Ruzmetov, D.; Zhang, K.; Stan, G.; Kalanyan, B.; Bhimanapati, G. R.; Eichfeld, S. M.; Burke, R. A.; Shah, P. B.; O'Regan, T. P.; Crowne, F. J., Vertical 2D/3D semiconductor heterostructures

based on epitaxial molybdenum disulfide and gallium nitride. Acs Nano 2016, 10 (3), 3580-3588.

23. Liao, J.; Sa, B.; Zhou, J.; Ahuja, R.; Sun, Z., Design of high-efficiency visible-light photocatalysts for water splitting: MoS2/AlN (GaN) heterostructures. The Journal of Physical Chemistry C 2014, 118 (31), 17594-17599.
24. Jeong, H.; Bang, S.; Oh, H. M.; Jeong, H. J.; An, S.-J.; Han, G. H.; Kim, H.; Kim, K. K.; Park, J. C.; Lee, Y. H., Semiconductor–insulator–semiconductor diode consisting of monolayer MoS2, h-BN, and GaN heterostructure. Acs Nano 2015, 9 (10), 10032-10038.
25. Lee, E. W.; Lee, C. H.; Paul, P. K.; Ma, L.; McCulloch, W. D.; Krishnamoorthy, S.; Wu, Y.; Arehart, A. R.; Rajan, S., Layer-transferred MoS2/GaN PN diodes. Appl Phys Lett 2015, 107 (10), 103505.
26. Tangi, M.; Mishra, P.; Ng, T. K.; Hedhili, M. N.; Janjua, B.; Alias, M. S.; Anjum, D. H.; Tseng, C.-C.; Shi, Y.; Joyce, H. J., Determination of band offsets at GaN/single-layer MoS2 heterojunction. Appl Phys Lett 2016, 109 (3), 032104.
27. Nourbakhsh, A.; Zubair, A.; Dresselhaus, M. S.; Palacios, T. s., Transport properties of a MoS2/WSe2 heterojunction transistor and its potential for application. Nano Lett 2016, 16 (2), 1359-1366.
28. Roy, T.; Tosun, M.; Cao, X.; Fang, H.; Lien, D.-H.; Zhao, P.; Chen, Y.-Z.; Chueh, Y.-L.; Guo, J.; Javey, A., Dual-gated MoS2/WSe2 van der Waals tunnel diodes and transistors. Acs Nano 2015, 9 (2), 2071-2079.
29. Lee, C.-H.; Lee, G.-H.; Van Der Zande, A. M.; Chen, W.; Li, Y.; Han, M.; Cui, X.; Arefe, G.; Nuckolls, C.; Heinz, T. F., Atomically thin p–n junctions with van der Waals heterointerfaces. Nature nanotechnology 2014, 9 (9), 676.
30. Aftab, S.; Khan, M. F.; Min, K.-A.; Nazir, G.; Afzal, A. M.; Dastgeer, G.; Akhtar, I.; Seo, Y.; Hong, S.; Eom, J., Van der Waals heterojunction diode composed of WS2 flake placed on p-type Si substrate. Nanotechnology 2017, 29 (4), 045201.
31. Yu, Y.; Fong, P. W.; Wang, S.; Surya, C., Fabrication of WS 2/GaN pn Junction by Wafer-Scale WS 2 Thin Film Transfer. Sci Rep-Uk 2016, 6, 37833.
32. Zhao, Z. H.; Wu, D.; Guo, J. W.; Wu, E. P.; Jia, C.; Shi, Z. F.; Tian, Y. T.; Li, X. J.; Tian, Y. Z., Synthesis of large-area 2D WS2 films and fabrication of a heterostructure for self-powered ultraviolet photodetection and imaging applications. J Mater Chem C 2019, 7 (39), 12121-12126.
33. Tang, H.; Zhang, H.; Chen, X.; Wang, Y.; Zhang, X.; Cai, P.; Bao, W., Recent progress in devices and circuits based on wafer-scale transition metal dichalcogenides. Science China Information Sciences 2019, 62 (12), 220401.
34. Zavabeti, A.; Jannat, A.; Zhong, L.; Haidry, A. A.; Yao, Z.; Ou, J. Z., Two-Dimensional Materials in Large-Areas: Synthesis, Properties and Applications. Nano-Micro Lett 2020, 12 (1), 1-34.
35. Brent, J. R.; Savjani, N.; O'Brien, P., Synthetic approaches to two-dimensional transition metal dichalcogenide nanosheets. Prog Mater Sci 2017, 89, 411-478.
36. Cai, Z.; Liu, B.; Zou, X.; Cheng, H.-M., Chemical vapor deposition growth and applications of two-dimensional materials and their heterostructures. Chemical reviews 2018, 118 (13), 6091-6133.
37. Wong, S. L.; Liu, H.; Chi, D., Recent progress in chemical vapor deposition growth of two-dimensional transition metal dichalcogenides. Progress in Crystal Growth and Characterization of Materials 2016, 62 (3), 9-28.
38. Koçak, Y.; Gür, E., Growth control of WS2; from 2D layer by layer to 3D vertical standing Nano-Walls. Acs Appl Mater Inter 2020.
39. Berkdemir, A.; Gutiérrez, H. R.; Botello-Méndez, A. R.; Perea-López, N.; Elías, A. L.; Chia, C.-I.; Wang, B.; Crespi, V. H.; López-Urías, F.; Charlier, J.-C., Identification of individual and few layers of WS 2 using Raman spectroscopy. Sci Rep-Uk 2013, 3 (1), 1-8.
40. Gora, V.; Chawanda, A.; Nyamhere, C.; Auret, F. D.; Mazunga, F.; Jaure, T.; Chibaya, B.; Omotoso, E.; Danga, H. T.; Tunhuma, S. M., Comparison of nickel, cobalt, palladium, and tungsten Schottky contacts on n-4H-silicon carbide. Physica B: Condensed Matter 2018, 535, 333-337.